

Triboelectric Materials

Core-Shell ZnO@Microporous Organic Polymer Nanospheres as Enhanced Piezo-Triboelectric Energy Harvesting Materials

Chang Wan Kang⁺, Dong-Min Lee⁺, Jina Park, Sohee Bang, Sang-Woo Kim,^{*} and Seung Uk Son^{*}

Abstract: Core-shell nanospheres were prepared by the homogeneous coating of piezoelectric ZnO nanorod aggregates with triboelectric microporous organic polymer (MOP). The small energy harvesting performance of ZnO@MOP was significantly enhanced, compared with those of ZnO and MOP, due to the piezoelectrification-induced polarization of inner ZnO and the enhanced generation of tribopositive charges of MOP. Piezo-triboelectric nanogenerators (PTENGs) fabricated with ZnO@MOP showed peak-to-peak voltages of up to 534 V and a maximum power density of 1.19 mW cm⁻². In addition, the PTENGs showed excellent durability for 30000 cycles, demonstrating as efficient power sources for charging electrolytic capacitors and for operating 200 green light emitting diode bulbs.

As energy concerns become more and more important in modern society, energy management-related technologies are attracting considerable attention from scientists.^[1] In this regard, small energy harvesting and utilization has been an important research subject.^[2] Various small energy sources such as mechanical stress and friction are available in common life and can be converted into electric power based on piezoelectric and triboelectric effects to operate electronic devices.^[3] Recently, there has been great progress in the development of small energy harvesting materials and devices.^[2-4]

Piezoelectric energy is generated through the mechanical stress-induced polarization of materials.^[5] In 2006, Wang et al. reported piezoelectric nanogenerators (PENGs) based on ZnO nanowire arrays.^[6] In comparison, triboelectric energy is generated by the friction-induced surface charges between two materials.^[7] In 2012, Wang et al. showed the

engineering of triboelectric nanogenerators (TENGs) using Kapton and polyethylene terephthalate polymers.^[8] Since then, various triboelectric polymer materials and TENGs have been developed.^[9]

Recently, piezo-triboelectric nanogenerators (PTENGs) with various piezo-triboelectric composite materials have been reported to enhance small energy harvesting performance.^[10] It is noteworthy that the triboelectric performance of PTENGs can be significantly enhanced by the piezoelectric effect in piezo-triboelectric composite materials.^[11]

Microporous organic polymers (MOPs) are versatile materials, due to their high surface areas and chemical stability.^[12] The MOPs have been prepared by coupling reactions of organic building blocks. Our research group has shown that morphologies of MOPs can be engineered using hard templates such as silica spheres and metal oxide nanoparticles.^[13] In addition, we have recently reported that Sonogashira coupling-based MOPs can be utilized as tribo-positive materials to harvest triboelectric energy, showing peak-to-peak voltages (V_{pp}) of up to 411 V and a maximum power density (P_{max}) of 0.80 mW cm⁻².^[14] We thought that multifunctional energy harvesting materials can be engineered by coating ZnO nanomaterials with MOP. In addition, the unprecedented energy harvesting performance of core-shell ZnO@MOP can be achieved through the possible piezoelectrification-assisted triboelectric effect. It is also noteworthy that while PTENGs have utilized the mixtures of piezoelectric nanomaterials and triboelectric polymers,^[10,11] as far as we are aware, the systems with core-shell materials have not been reported. In this work, we report template synthesis of core-shell ZnO@MOP and its small energy harvesting performance.

Figure 1 shows the engineering of ZnO, ZnO@MOP, MOP, and their films using polyvinylpyrrolidone (PVP) as a matrix. ZnO nanospheres were prepared by a synthetic method reported in the literature.^[15] The Sonogashira coupling of tetra(4-ethynylphenyl)methane with 1,4-diiodobenzene in the presence of ZnO nanospheres resulted in the homogeneous coating of ZnO with MOP to form ZnO@MOP. The acid etching of inner ZnO from ZnO@MOP generated hollow MOP materials.

The morphologies of ZnO, ZnO@MOP, and MOP powders were investigated by scanning (SEM) and transmission electron microscopy (TEM) (Figures 2 and S1 in the Supporting Information). The SEM images of ZnO powder show a spherical shape with an average diameter of 440 ± 45 nm (Figures 2a and 2d). TEM analysis showed that the

[*] Dr. C. W. Kang,⁺ J. Park, S. Bang, Prof. S. U. Son
 Department of Chemistry,
 Sungkyunkwan University
 Suwon 16419 (Korea)
 E-mail: sson@skku.edu

D.-M. Lee,⁺ Prof. S.-W. Kim
 School of Advanced Materials Science and Engineering,
 Sungkyunkwan University
 Suwon 16419 (Korea)
 E-mail: kimsu1@skku.edu

[†] These authors contributed equally to this work.

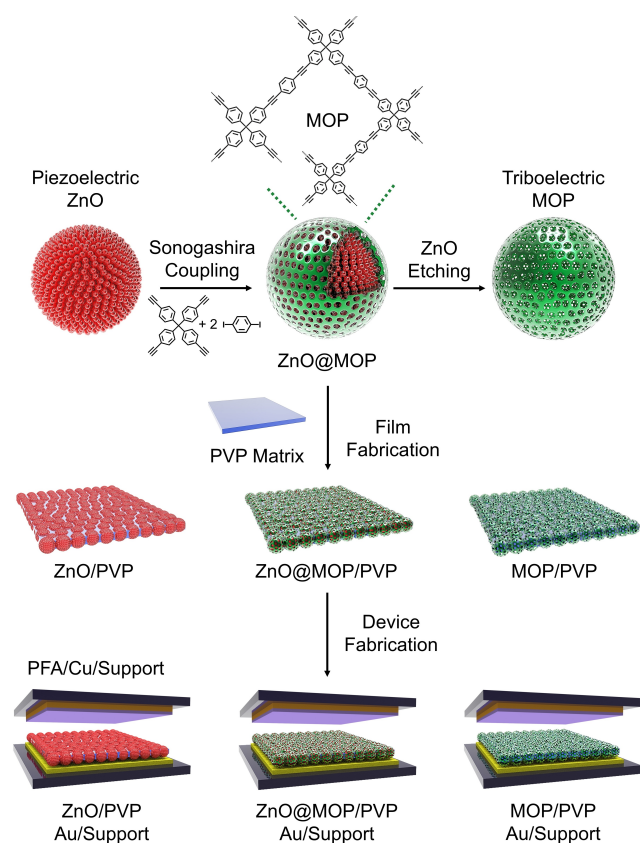


Figure 1. Synthesis of ZnO, ZnO@MOP, and MOP and the engineering of thin films of ZnO, ZnO@MOP, and MOP in the PVP matrix.

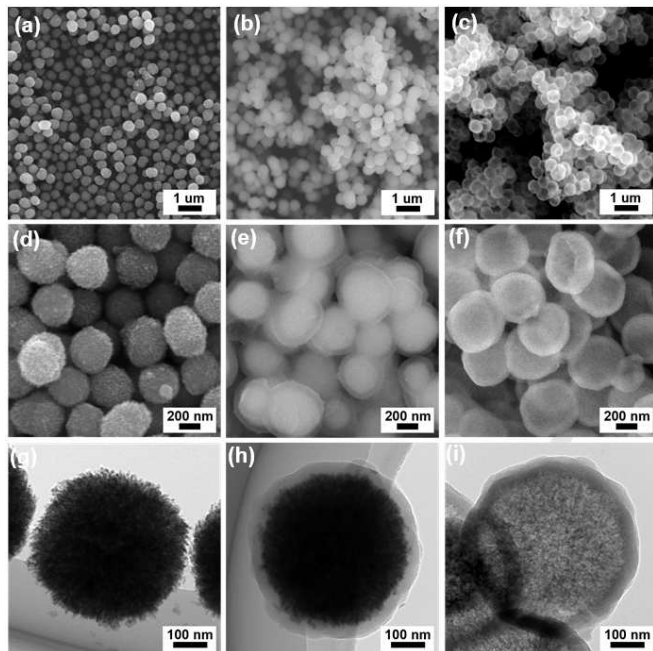


Figure 2. SEM images of a, d) ZnO, b, e) ZnO@MOP, and c, f) MOP. TEM images of g) ZnO, h) ZnO@MOP, and i) MOP.

ZnO nanospheres consist of small rods with a thickness of 10–15 nm and a length of 50–70 nm (Figure 2g). The diameter of ZnO@MOP increased to 531 ± 35 nm, due to the homogeneous coating of ZnO nanospheres with MOP (Figures 2b, 2e, and 2h). The MOP showed a hollow morphology with an average diameter of 531 ± 40 nm and an average shell thickness of 44 ± 4 nm (Figures 2c, 2f, and 2i).

The chemical components of ZnO, ZnO@MOP, and MOP were characterized by powder X-ray diffraction studies (PXRD), infrared absorption (IR), and solid state ^{13}C nuclear magnetic resonance (NMR) spectroscopy. The PXRD pattern of ZnO showed diffraction peaks at 2θ of 31.8, 34.5, 36.2, 47.5, 56.6, 62.9, and 68.2°, corresponding to the (100), (002), (101), (102), (110), (103), and (112) crystalline planes of hexagonal wurtzite ZnO (JCPDS# 36-1451) (Figure 3a). ZnO@MOP maintained the original wurtzite structure of ZnO, indicating that during the MOP coating, the crystalline structure of ZnO was not changed. MOP showed an amorphous feature, matching well with the MOP materials reported in the literature.^[12,13] The IR spectrum of ZnO showed the Zn–O vibration peak at 502 cm^{-1} , in addition to surface O–H stretching at 3433, 1561, and 1417 cm^{-1} (Figure 3b). MOP showed aromatic C=C and C–H vibration peaks at 1510 and 822 cm^{-1} , respectively. As expected, the IR spectrum of ZnO@MOP showed the mixed IR peaks of ZnO and MOP. The solid state ^{13}C NMR spectrum of MOP showed the aromatic ^{13}C peaks at 145, 136, 130, and 121 ppm (Figure 3c). In addition,

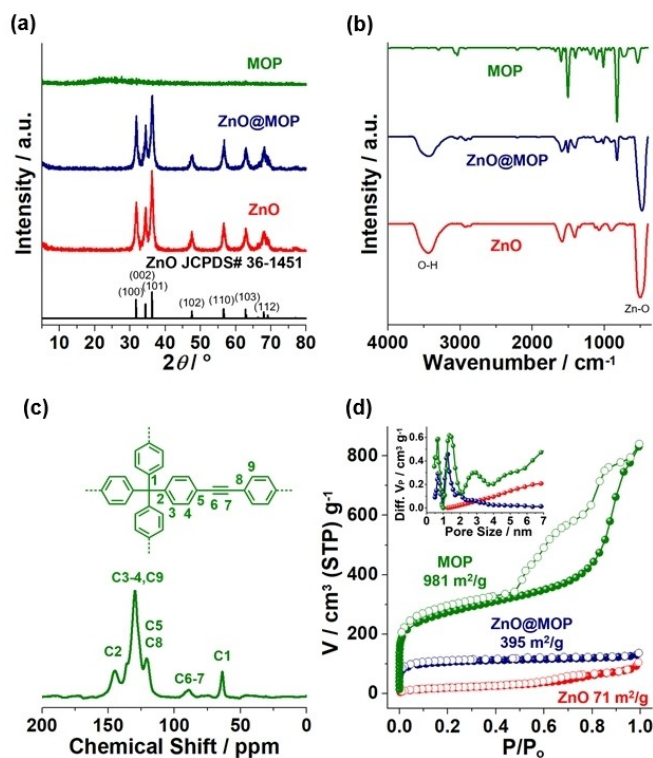


Figure 3. a) PXRD patterns of MOP, ZnO@MOP, and ZnO. b) IR spectra of MOP, ZnO@MOP, and ZnO. c) Solid state ^{13}C NMR spectrum of MOP. d) N_2 adsorption-desorption isotherm curves at 77 K and pore size distribution diagrams based on the DFT method.

the ^{13}C peaks of alkyne and benzyl carbon were observed at 90 and 64 ppm, respectively, indicating that the MOP materials were formed by the Sonogashira coupling of the used building blocks.^[13]

The surface areas and porosity of ZnO, ZnO@MOP, and MOP were investigated by analysis of the N_2 adsorption-desorption curves based on Brunauer–Emmett–Teller (BET) theory (Figure 3d). The surface area of ZnO was measured to be $71\text{ m}^2\text{ g}^{-1}$, showing mesoporosity with an average pore diameter of 7.5 nm. The mesopores of ZnO originated from the inter-rod space of ZnO rods. The ZnO@MOP showed a sharp increase of the surface area to $395\text{ m}^2\text{ g}^{-1}$ with microporosity (pore sizes $<2\text{ nm}$), indicating the successful formation of MOP on the ZnO spheres. The MOP showed a high surface area of $981\text{ m}^2\text{ g}^{-1}$ with both mesoporous and microporous features. The microporosity and mesoporosity of MOP originated from organic networks and the space of etched ZnO rods, respectively.

Figure 4a shows the fabrication process of thin films bearing ZnO@MOP in a PVP matrix. After ZnO@MOP powder was added to ethanol, the mixture was well ground (Steps 1–2 in Figure 4a). After PVP in ethanol was added, the mixture was stirred (Step 3 in Figure 4a). Using a doctor blade, a film with a thickness of $30\text{ }\mu\text{m}$ was fabricated and dried (Steps 4–7 in Figure 4a). Finally, the film was cut to pieces with an area of $2\text{ cm}\times 2\text{ cm}$. The contents of ZnO, ZnO@MOP, and MOP in the PVP matrix gradually

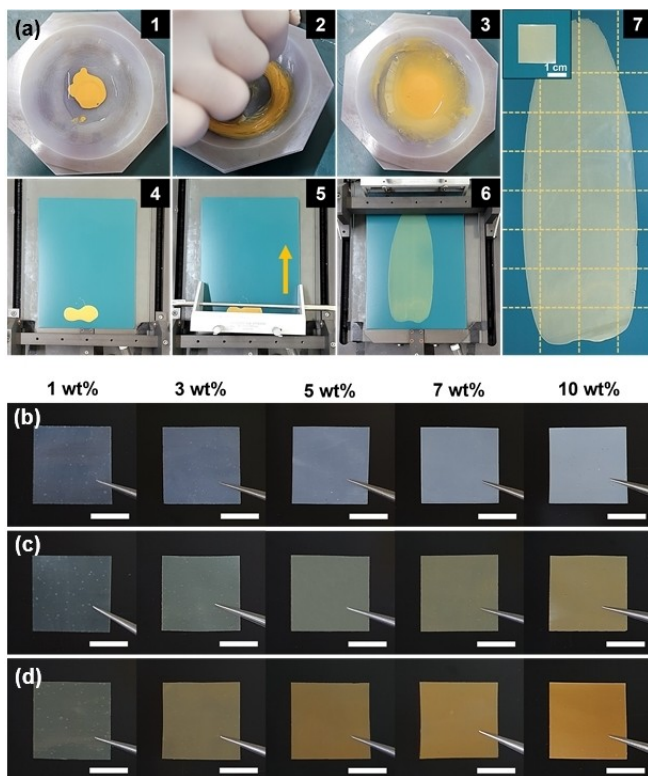


Figure 4. a) Fabrication processes of a 7 wt% ZnO@MOP/PVP film. Photographs of b) 1, 3, 5, 7, & 10 wt% ZnO/PVP, c) 1, 3, 5, 7, & 10 wt% ZnO@MOP/PVP, and d) 1, 3, 5, 7, & 10 wt% MOP/PVP films (scale bar: 1 cm).

increased from 1 wt % to 3, 5, 7, and 10 wt % to prepare five films of each material (Figures 4b–d and S2 in the Supporting Information). When the content of additive materials exceeded 10 wt %, free standing films could not be obtained. The thickness of all films was measured to be $\approx 30\text{ }\mu\text{m}$ by a caliper.

Using perfluoroalkoxy alkanes (PFA, thickness of $25\text{ }\mu\text{m}$) as counting tribonegative materials,^[16] the piezotriboelectrification performance of ZnO/PVP, ZnO@MOP/PVP, and MOP/PVP films were investigated with a mechanical pusher (relative humidity, RH: 50%, pushing force: 2 kgf, frequency: 0.75 Hz). Figures 5, 7, and S3 in the Supporting Information summarize the results. As the content of ZnO in ZnO/PVP films increased from 0 wt % to 1, 3, 5, 7, and 10 wt %, the V_{pp} increased and then slightly decreased from 246 V to 292, 309, 320, 320, and 312 V, respectively (Figure 5a). In comparison, as the content of MOP in MOP/PVP films increased from 1 wt % to 3, 5, 7, and 10 wt %, the V_{pp} gradually increased and then slightly decreased from 374 V to 395, 413, 409, and 404 V (Figure 5a). Interestingly, ZnO@MOP/PVP films showed the

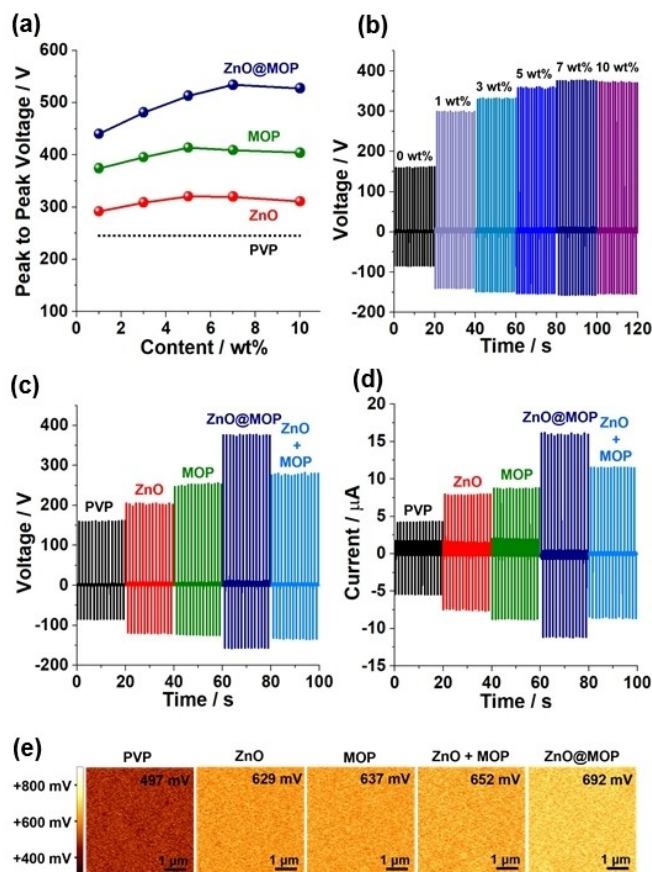


Figure 5. a) Output peak-to-peak voltages (V_{pp}) of small energy harvesters with PVP, 1–10 wt % ZnO/PVP, 1–10 wt % MOP/PVP, 1–10 wt % ZnO@MOP/PVP films (working area of $2\text{ cm}\times 2\text{ cm}$, pushing force of 2 kgf, 0.75 Hz, RH: 50%). b) Output voltages of small energy harvesters with 1–10 wt % ZnO@MOP/PVP films. c) Output voltages and d) currents of small energy harvesters with PVP, 5.6 wt % ZnO, 1.4 wt % MOP, 5.6 wt % ZnO + 1.4 wt % MOP/PVP, and 7 wt % ZnO@MOP/PVP films and e) KPFM images of films.

best small energy harvesting performance with higher V_{pp} values. As the content of ZnO@MOP in ZnO@MOP/PVP films increased from 1 wt % to 3, 5, 7, and 10 wt %, the V_{pp} increased and then decreased from 440 V to 481, 513, 534, and 528 V (Figures 5a–b). As pushing force increased from 0.5 kgf to 1.0, 1.5, 2.0, and 2.5 kgf, the V_{pp} of 7 wt % ZnO@MOP/PVP films increased gradually from 245 V to 361, 453, 534, and 598 V (Figure S4 in the Supporting Information). In comparison, when pushing frequency (pushing force: 2 kgf) increased from 0.23 Hz to 2.75 Hz, the V_{pp} of 7 wt % ZnO@MOP/PVP films retained in the range of 534–535 V (Figure S4 in the Supporting Information).

By gravimetric analysis, the contents of ZnO and MOP in ZnO@MOP were analyzed to be 80 and 20 wt %, respectively. For control tests, 5.6 wt % ZnO/PVP, 1.4 wt % MOP/PVP, and 5.6 wt % ZnO + 1.4 wt % MOP/PVP films were prepared and their small energy harvesting performance was compared with those of 7 wt % ZnO@MOP/PVP and control PVP films (Figures 5c–d and S5 in the Supporting Information). The V_{pp} values increased in the order of PVP < 5.6 wt % ZnO/PVP < 1.4 wt % MOP/PVP < 5.6 wt % ZnO + 1.4 wt % MOP/PVP < 7 wt % ZnO@MOP/PVP with 246, 326, 380, 416, and 534 V, respectively. The corresponding peak-to-peak currents (I_{pp}) of PVP, 5.6 wt % ZnO/PVP, 1.4 wt % MOP/PVP, 5.6 wt % ZnO + 1.4 wt % MOP/PVP, and 7 wt % ZnO@MOP/PVP films increased from 9.8 μ A to 15.5, 17.5, 20.2, and 26.8 μ A, respectively (Figure 5d). By Kelvin probe force microscopy (KPFM, AC voltage: 2 V), the surface potentials of PVP, 5.6 wt % ZnO/PVP, 1.4 wt % MOP/PVP, 5.6 wt % ZnO + 1.4 wt % MOP/PVP, and 7 wt % ZnO@MOP/PVP films gradually increased from 497 mV to 629, 637, 652, and 692 mV, respectively, matching well with their trend of small energy harvesting performance (Figure 5e). These results indicate that ZnO@MOP is a more efficient small energy harvesting material than ZnO nanospheres or MOP.

According to the water contact angle (WCA) studies, whilst ZnO powder was hydrophilic with a WCA of 47°, MOP and ZnO@MOP powders were hydrophobic with WCAs of 134 and 110°, respectively. While a WCA of the 5.6 wt % ZnO/PVP film was 65°, that of the 5.6 wt % ZnO + 1.4 wt % MOP/PVP film was 85°. In comparison, a WCA of the 7 wt % ZnO@MOP/PVP film was 98°, due to efficient coating of hydrophilic ZnO particles with hydrophobic MOP (Figure S6 in the Supporting Information). This can be one of the reasons for the better small energy harvesting performance of the 7 wt % ZnO@MOP/PVP film, compared with the 5.6 wt % ZnO + 1.4 wt % MOP/PVP film. When a moisture effect was tested, the 7 wt % ZnO@MOP/PVP film maintained similar performance in the RH range of 30–50 % with output V_{pp} of 534–555 V. In comparison, when RH increased to 80 %, the performance of the 7 wt % ZnO@MOP/PVP film significantly decreased with output V_{pp} of 133 V (Figure S7 in the Supporting Information).

A small energy harvesting mechanism was suggested in Figure 6.^[17] It can be speculated that basically, TENG would work in all combinations of tribopositive PVP, ZnO/PVP, MOP/PVP, and ZnO@MOP/PVP films with tribonegative PFA. When tribopositive films are in contact with a tribo-

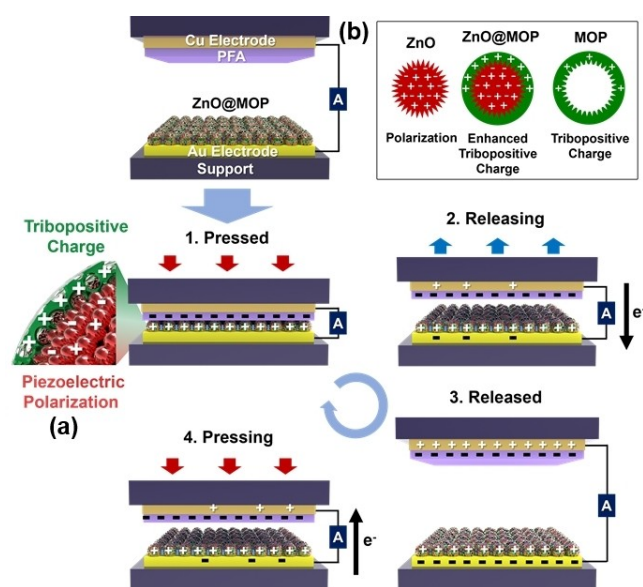


Figure 6. a) A small energy harvesting mechanism of PTENG fabricated with ZnO@MOP/PVP and PFA films. b) The mechanical stress-induced piezoelectric or triboelectric charges of ZnO, ZnO@MOP, and MOP.

negative PFA film, charge transfer occurs at their interface. In a releasing step, electrons flow from the PFA-loaded Cu electrode to the tribopositive film-loaded Au electrode. In the following pressing step after the fully released step, electrons flow from Au electrode to Cu electrode. Then, the contact and release processes are cycled (Figure 6a). In the combinations of PVP and PFA films, triboelectrification occurs between tribopositive PVP and tribonegative PFA. It is noteworthy that the ZnO/PVP film showed enhanced TENG performance, compared with that of the PVP film. In the combination of MOP/PVP and PFA films, the MOP acts as the better tribopositive material than PVP (Figure 5).^[14] In the combination of ZnO@MOP/PVP and PFA films, basically, the MOP shells would act as tribopositive materials. It has been reported that the TENG performance of polymers in PTENG can be significantly enhanced with the help of piezoelectric ZnO or BaTiO₃.^[10,11] In this regard, we suggest that the piezoelectrification-induced polarization of ZnO rods enhances the triboelectrification of MOP in ZnO@MOP on the surface or near surface of ZnO@MOP/PVP films (Figures S8–S9 in the Supporting Information).^[6,11] Figure 6b displays the press-induced piezoelectric or triboelectric charges of ZnO, ZnO@MOP, and MOP materials.

To investigate the facilitated polarization degree of materials, their relative permittivities (ϵ_r) were characterized by measuring the charge capacitances of PVP, ZnO/PVP, MOP/PVP, and ZnO@MOP/PVP films, (Figure S10 in the Supporting Information).^[18] The ϵ_r (24.8) of the 7 wt % ZnO@MOP/PVP film was much higher than those of PVP (4.2), 5.6 wt % ZnO/PVP (8.7), 1.4 wt % MOP/PVP (7.7), and 5.6 wt % ZnO + 1.4 wt % MOP/PVP (13.7) films. These results confirm that the charge storage performance of the

ZnO@MOP/PVP film can be much enhanced, compared with those of ZnO/PVP and MOP/PVP films, matching well with the observed trend of small energy harvesting performance.

Next, the long cycling performance of PTENG with a 7 wt % ZnO@MOP/PVP film was investigated. Figure 7a shows excellent durability of PTENG with a 7 wt % ZnO@MOP/PVP film during 30000 cycles, maintaining the V_{pp} in the range of 534–540 V. It is noteworthy that whilst ZnO@MOP was thermally stable up to 330 °C, the 7 wt % ZnO@MOP/PVP film showed Young's modulus of 1.87 GPa with maximum tensile strength of 37.3 MPa (Figures S11–12 in the Supporting Information). Figure 7b shows the resistance-dependent current and power densities of PTENG with a 7 wt % ZnO@MOP/PVP film, displaying the current densities of 77, 69, 60, 35, and 8.6 mA/m² at the resistances

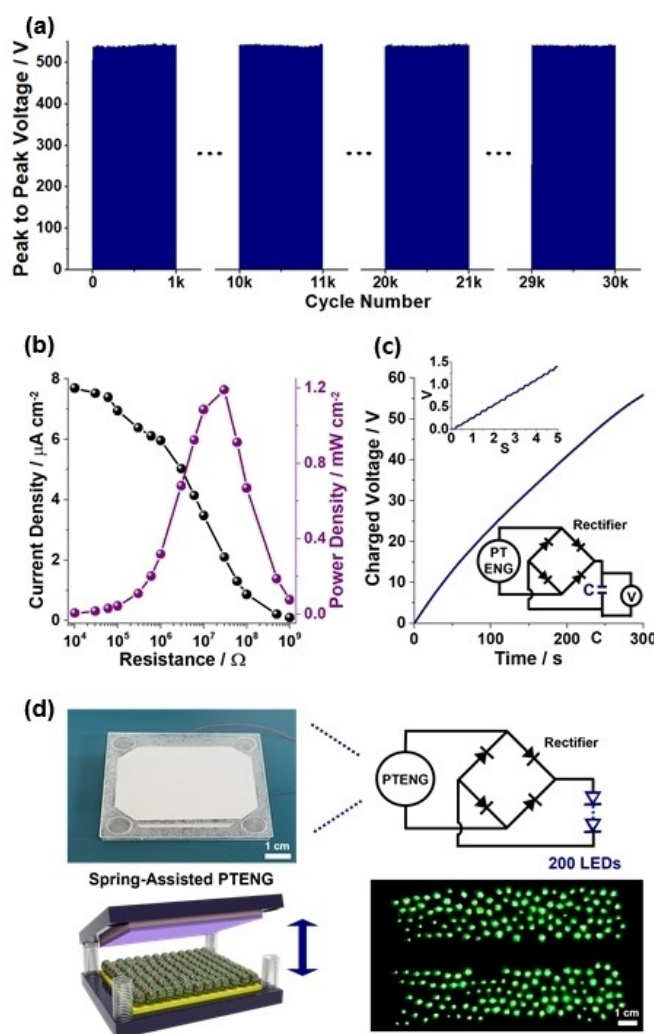


Figure 7. a) Cycling performance (working area of 2 cm × 2 cm, pushing force of 2 kgf, frequency of 0.75 Hz), b) resistance dependent current and power densities, and power source demonstrations (working area of 3 cm × 3 cm, pushing force of 1 kgf, frequency of 3.5 Hz) for c) charging of a capacitor (4.7 µF Al electrolytic capacitor) and for d) operation of 200 green LEDs (photon, PV525-5A5D-NNISLA-Z) of PTENG with a 7 wt % ZnO@MOP/PVP film.

of 10⁴, 10⁵, 10⁶, 10⁷, and 10⁸ Ω, respectively, and the P_{max} of 1.19 mW cm⁻² at the resistance of 3 × 10⁷ Ω.

A spring-incorporated PTENG with a 7 wt % ZnO@MOP/PVP film was fabricated and tested as a power source for the charging capacitor^[19] and the operation of LEDs and a low-power electronic device^[20] (Figures 7c–d and S13 in the Supporting Information). When the PTENG with a 7 wt % ZnO@MOP/PVP film was operated with pushing force of 1 kgf and frequency of 3.5 Hz, the charged voltages of 15.2 and 55.9 V of an electrolytic capacitor (4.7 µF) were obtained within 1 and 5 min, respectively. In addition, the PTENG was successfully demonstrated as a power source to operate 200 green LEDs and a low-powered electronic device (Movies S1–3 in the Supporting Information).

The piezo-triboelectric energy harvesting performance of a 7 wt % ZnO@MOP/PVP film was compared with the conventional polymer films and recent materials in the literature (Figure S14 and Table S1–2 in the Supporting Information).^[10,11,14,21] First, whilst the MOP-based TENGs showed V_{pp} of 411 V and P_{max} of 0.80 mW cm⁻² in our previous report, the PTENG with a 7 wt % ZnO@MOP/PVP film in this work showed V_{pp} of 534 V and P_{max} of 1.19 mW cm⁻².^[14] It is noteworthy that the 7 wt % ZnO@MOP/PVP film was more tribopositive than commercial nylon, polyurethane, poly(vinyl alcohol), and poly(methyl methacrylate) films (Figure S14 in the Supporting Information). Second, the small energy harvesting performance of PTENG in this work is superior to, or comparable with, those of the recent polymer-based TENGs (Table S1 in the Supporting Information).^[21] For example, the TENGs with polypyrrole, silk fibroin, chitosan, poly(lactic acid), and polyurethane were fabricated in the literature, displaying P_{max} of 0.013–0.55 mW cm⁻².^[21a–j] In addition, the silicon-nylon composite-based TENGs showed P_{max} of 1.12 mW cm⁻².^[21k] Third, the small energy harvesting performance of PTENG with a 7 wt % ZnO@MOP/PVP film in this work is superior to, or comparable with, those of recent PTENGs with the mixtures of piezoelectric ZnO or BaTiO₃ (BTO) with triboelectric polymeric materials in the literature (Table S2 in the Supporting Information).^[10,11] For example, in 2021, Yu et al. reported PTENGs with a composite of ZnO microflowers and polydimethylsiloxane (PDMS), showing V_{pp} of 247 V and P_{max} of 0.6 mW cm⁻².^[11j] In 2021–2022, Vittayakorn, Kim, Pan et al. reported the PTENGs based on BTO and chitosan, PDMS, and polyvinylidene fluoride (PVDF), displaying V_{pp} of 111–444 V and P_{max} of 0.04–0.76 mW cm⁻².^[11k–m] While the PTENGs in the literature are based on the conventional mixture of ZnO or BTO with triboelectric polymers, the studies utilizing core–shell material have not been reported.^[10,11] We suggest that the core–shell structure can efficiently enhance the triboelectrification of MOP shells through the assistance of core ZnO materials, due to the piezoelectrification-induced polarization of core ZnO, the technical blocking of ZnO aggregations by MOP coating, the efficient contact of core and shell materials, and the hydrophobic coating of hydrophilic ZnO materials.

In conclusion, this work introduces new piezo-triboelectric hybrid materials based on core–shell ZnO@MOP

materials. The MOP shells were introduced by the Sonogashira coupling of organic building blocks in the presence of ZnO nanoparticles. The core-shell ZnO@MOP materials showed efficient small energy harvesting performance in PTENG, due to the enhanced triboelectrification performance of MOP shells by the assistance of piezoelectric ZnO materials. We believe that various piezoelectric core-triboelectric MOP shells can be developed by the screening of inorganic core materials and the organic building blocks for MOP shells.

Acknowledgements

This work was supported by the National Research Foundation of Korea (NRF) grant (No. 2020R1A2C2004310 and No. 2022R1A3B1078291) funded by the Korea government (MSIT).

Conflict of Interest

The authors declare no conflict of interest.

Data Availability Statement

The data that support the findings of this study are available from the corresponding author upon reasonable request.

Keywords: Microporous Organic Polymer · Piezoelectric Energy · Small Energy Harvesting · Triboelectric Energy · Zinc Oxide

- [1] a) G. Chen, Y. Li, M. Bick, J. Chen, *Chem. Rev.* **2020**, *120*, 3668–3720; b) M. Gao, P. Wang, L. Jiang, B. Wang, Y. Yao, S. Liu, D. Chu, W. Cheng, Y. Lu, *Energy Environ. Sci.* **2021**, *14*, 2114–2157; c) L. Yin, K. N. Kim, A. Trifonov, T. Podhajny, J. Wang, *Energy Environ. Sci.* **2022**, *15*, 82–101.
- [2] a) Z. L. Wang, *Adv. Energy Mater.* **2020**, *10*, 2000137; b) C. Huang, G. Chen, A. Nashalian, J. Chen, *Nanoscale* **2021**, *13*, 2065–2081; c) M. Yan, Z. Xiao, J. Ye, X. Xuan, Z. Li, C. Bowen, Y. Zhang, D. Zhang, *Energy Environ. Sci.* **2021**, *14*, 6158–6190.
- [3] a) C. Rodrigues, D. Nunes, D. Clemente, N. Mathias, J. M. Correia, P. Rosa-Santos, F. Taveira-Pinto, T. Morais, A. Pereira, J. Ventura, *Energy Environ. Sci.* **2020**, *13*, 2657–2683; b) J. Lv, L. Jeerapan, F. Tehrani, L. Yin, C. A. Silva-Lopez, J.-H. Jang, D. Joshua, R. Shah, Y. Liang, L. Xie, F. Soto, C. Chen, E. Karshalev, C. Kong, Z. Yang, J. Wang, *Energy Environ. Sci.* **2018**, *11*, 3431–3442; c) C. R. Bowen, J. Taylor, E. LeBoulbar, D. Zabek, A. Chauhan, R. Vaish, *Energy Environ. Sci.* **2014**, *7*, 3836–3856.
- [4] a) D. W. Kim, J. H. Lee, J. K. Kim, U. Jeong, *NPG Asia Mater.* **2020**, *12*, 6; b) X. Zhang, L. Chen, Y. Jiang, W. Lim, S. Soh, *Chem. Mater.* **2019**, *31*, 1473–1478; c) N. A. Shepelin, A. M. Glushenkov, V. C. Lussini, P. J. Fox, G. W. Dicoski, J. G. Shapter, A. V. Ellis, *Energy Environ. Sci.* **2019**, *12*, 1143–1176.
- [5] N. Sezer, M. Koç, *Nano Energy* **2021**, *80*, 105567.
- [6] Z. L. Wang, J. Song, *Science* **2006**, *312*, 242–246.
- [7] a) C. Wu, A. C. Wang, W. Ding, H. Guo, Z. L. Wang, *Adv. Energy Mater.* **2019**, *9*, 1802906; b) Z. L. Wang, *Mater. Today* **2017**, *20*, 74–82.
- [8] F.-R. Fan, Z.-Q. Tian, Z. L. Wang, *Nano Energy* **2012**, *1*, 328–334.
- [9] Teng polymer A. Chen, C. Zhang, G. Zhu, Z. L. Wang, *Adv. Sci.* **2020**, *7*, 2000186.
- [10] J. Zhang, Y. He, C. Boyer, K. Kalantar-Zadeh, S. Peng, D. Chu, C. H. Wang, *Nanoscale Adv.* **2021**, *3*, 5465–5486.
- [11] a) G. Wang, Y. Xi, H. Xuan, R. Liu, X. Chen, L. Cheng, *Nano Energy* **2015**, *18*, 28–36; b) X. Yang, W. A. Daoud, *Adv. Funct. Mater.* **2016**, *26*, 8194–8201; c) B. Shi, Q. Zheng, W. Jiang, L. Yan, X. Wang, H. Liu, Y. Yao, Z. Li, Z. L. Wang, *Adv. Mater.* **2016**, *28*, 846–852; d) D. H. Kim, B. Dudem, J. S. Yu, *ACS Sustainable Chem. Eng.* **2018**, *6*, 8525–8535; e) W. He, Y. Qian, B. S. Lee, F. Zhang, A. Rasheed, J.-E. Jung, D. J. Kang, *ACS Appl. Mater. Interfaces* **2018**, *10*, 44415–44420; f) Y. Qian, D. J. Kang, *ACS Appl. Mater. Interfaces* **2018**, *10*, 32281–32288; g) H. H. Singh, N. Khare, *Nano Energy* **2018**, *51*, 216–222; h) Y. Wu, J. Qu, W. A. Daoud, L. Wang, T. Qi, *J. Mater. Chem. A* **2019**, *7*, 13347–13355; i) S. Sriphan, T. Charoonsuk, T. Maluangnont, N. Vittayakorn, *ACS Appl. Energy Mater.* **2019**, *2*, 3840–3850; j) H. Patnam, S. A. Graham, J. S. Yu, *ACS Sustainable Chem. Eng.* **2021**, *9*, 4600–4610; k) S. Pongampai, T. Charoonsuk, N. Pinpru, P. Pulohol, W. Vittayakorn, P. Pakawanit, N. Vittayakorn, *Composites Part B* **2021**, *208*, 108602; l) M. Sahu, V. Vivekananthan, S. Hajra, D. K. Khatua, S.-J. Kim, *Appl. Mater. Today* **2021**, *22*, 100900; m) J.-H. Zhang, Z. Zhou, J. Li, B. Shen, T. Zhu, X. Gao, R. Tao, X. Guo, X. Hu, Y. Shi, L. Pan, *ACS Mater. Lett.* **2022**, *4*, 847–852; n) Z. Wang, Z. Liu, G. Zhao, Z. Zhang, X. Zhao, X. Wan, Y. Zhang, Z. I. Wang, L. Li, *ACS Nano* **2022**, *16*, 1661–1670.
- [12] a) J.-S. M. Lee, A. I. Cooper, *Chem. Rev.* **2020**, *120*, 2171–2214; b) D. Taylor, S. J. Dalgarno, Z. Xu, F. Vilela, *Chem. Soc. Rev.* **2020**, *49*, 3981–4042; c) J. Wu, F. Xu, S. Li, P. Ma, X. Zhang, Q. Liu, R. Fu, D. Wu, *Adv. Mater.* **2019**, *31*, 1802922; d) B. Zheng, X. Lin, X. Zhang, D. Wu, K. Matyjaszewski, *Adv. Funct. Mater.* **2019**, *30*, 1907006; e) N. Chaoui, M. Trunk, R. Dawson, J. Schmidt, A. Thomas, *Chem. Soc. Rev.* **2017**, *46*, 3302–3321; f) L. Tan, B. Tan, *Chem. Soc. Rev.* **2017**, *46*, 3322–3356; g) S. Das, P. Heasman, T. Ben, S. Qiu, *Chem. Rev.* **2017**, *117*, 1515–1563; h) J.-K. Sun, M. Antonietti, J. Yuan, *Chem. Soc. Rev.* **2016**, *45*, 6627–6656; i) Y. Xu, S. Jin, H. Xu, A. Nagai, D. Jiang, *Chem. Soc. Rev.* **2013**, *42*, 8012–8031; j) D. Wu, F. Xu, B. Sun, R. Fu, H. He, K. Matyjaszewski, *Chem. Rev.* **2012**, *112*, 3959–4015.
- [13] a) K. Cho, C. W. Kang, S. H. Ryu, J. Y. Jang, S. U. Son, *J. Mater. Chem. A* **2022**, *10*, 6950–6964; b) N. Kang, J. H. Park, M. Jin, N. Park, S. M. Lee, H. J. Kim, J. M. Kim, S. U. Son, *J. Am. Chem. Soc.* **2013**, *135*, 19115–19118.
- [14] S. I. Park, D.-M. Lee, C. W. Kang, S. M. Lee, H. J. Kim, Y.-J. Ko, S.-W. Kim, S. U. Son, *J. Mater. Chem. A* **2021**, *9*, 12560–12565.
- [15] D. Jézéquel, J. Guenot, N. Jouini, F. Fievet, *J. Mater. Res.* **1995**, *10*, 77–83.
- [16] R. Hinchet, H.-J. Yoon, H. Ryu, M.-K. Kim, E.-K. Choi, D.-S. Kim, S. W. Kim, *Science* **2019**, *365*, 491–494.
- [17] R. Hinchet, W. Seung, S.-W. Kim, *ChemSusChem* **2015**, *8*, 2327–2344.
- [18] a) J. Kim, H. Ryu, J. H. Lee, U. Khan, S. S. Kwak, H.-J. Yoon, S.-W. Kim, *Adv. Energy Mater.* **2020**, *10*, 1903524; b) S. K. Bhattacharya, J. Y. Park, R. R. Tummala, M. G. Allen, *J. Mater. Sci. Mater. Electron.* **2000**, *11*, 455–460.
- [19] S. Han, E. J. Lee, B. Kim, S. Jung, S. Jeong, S.-W. Kim, Y. Choi, S. Y. Lee, *ACS Energy Lett.* **2020**, *5*, 3507–3513.
- [20] H. Oh, S. S. Kwak, B. Kim, E. Han, G.-H. Lim, S.-W. Kim, B. Lim, *Adv. Funct. Mater.* **2019**, *29*, 1904066.

- [21] a) J. Wang, Z. Wen, Y. Zi, P. Zhou, J. Lin, H. Guo, Y. Xu, Z. L. Wang, *Adv. Funct. Mater.* **2016**, *26*, 1070–1076; b) X.-S. Zhang, J. Brugger, B. Kim, *Nano Energy* **2016**, *20*, 37–47; c) Q. Zheng, L. Fang, H. Guo, K. Yang, Z. Cai, M. A. B. Meador, S. Gong, *Adv. Funct. Mater.* **2018**, *28*, 1706365; d) R. Pan, W. Xuan, J. Chen, S. Dong, H. Jin, X. Wang, H. Li, J. Luo, *Nano Energy* **2018**, *45*, 193–202; e) C. Jiang, C. Wu, X. Li, Y. Yao, L. Lan, F. Zhao, Z. Ye, Y. Ying, J. Ping, *Nano Energy* **2019**, *59*, 268–276; f) F. Chen, Y. Wu, Z. Ding, X. Xia, S. Li, H. Zheng, C. Diao, G. Yue, Y. Zi, *Nano Energy* **2019**, *56*, 241–251; g) S. Yan, K. Dong, J. Lu, W. Song, R. Xiao, *Nanoscale* **2020**, *12*, 4527–4536; h) C. Park, M. Koo, G. Song, S. M. Cho, H. S. Kang, T. H. Park, E. H. Kim, C. Park, *ACS Nano* **2020**, *14*, 755–766; i) L. Zhang, Y. Liao, Y.-C. Wang, S. Zhang, W. Yang, X. Pan, Z. L. Wang, *Adv. Funct. Mater.* **2020**, *30*, 2001763; j) X. Zhao, D. Zhang, S. Xu, W. Qian, W. Han, Z. L. Wang, Y. Yang, *Nano Energy* **2020**, *75*, 104920; k) J. Qian, J. He, S. Qian, J. Zhang, X. Niu, X. Fan, C. Wang, X. Hou, J. Mu, W. Geng, X. Chou, *Adv. Funct. Mater.* **2020**, *30*, 1907414.

Manuscript received: July 1, 2022

Accepted manuscript online: September 21, 2022

Version of record online: October 18, 2022